Asian Journal of Chemistry; Vol. 35, No. 2 (2023), 435-440

ASIAN JOURNAL OF CHEMISTRY

https://doi.org/10.14233/ajchem.2023.26921

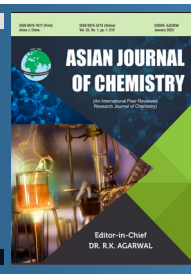

Synthesis of Ca-doped CeO_2 Nanoparticles for the Enhanced Adsorption Activity of Chitosan and Other Applications

M.P. GEETHA[1,*], R. NAZARETH[2], P. SURYA[1], P. PRATHEEKSHA[1] and P.A. SUCHETAN[3,*]

[1]Post Graduate Department of Chemistry, St. Agnes College, Mangaluru-575002, India
[2]Department of Chemistry, St Aloysius College (Autonomous), Mangaluru-575003, India
[3]Department of Studies and Research in Chemistry, University College of Science, Tumkur University, Tumakuru-572103, India

*Corresponding authors: E-mail: geetha@stagnescollege.edu.in; pasuchetan@gmail.com

Received: 29 October 2022; *Accepted*: 17 December 2022; *Published online*: 30 January 2023; AJC-21127

Calcium doped cerium oxide (CeO_2) nanoparticles (NPs) were synthesized by co-precipitation method with ammonium ceric sulfate as the precursor and ethanol as solvent. They were characterized through X-ray diffraction (XRD), scanning electron microscopy (SEM) and energy-dispersive X-ray (EDX) analyses. Pure CeO_2 NPs have a crystallite size of 9 nm, while, calcium-doped ones have 2 nm and are having regular spherical shapes. Brunauer-Emmett-Teller (BET) surface analysis indicated that calcium-doped CeO_2 NPs have larger specific surface area (59.806 m^2/g) than pure CeO_2 NPs (30-40 m^2/g). As a result, chitosan incorporated with calcium doped CeO_2 NPs showed better adsorption efficiencies (48-70%) than when incorporated with undoped CeO_2 NPs (35-51%). Studies suggested that calcium doped CeO_2 NPs are better potential photocatalyst for methyl orange degradation, with efficiencies between 25-68 % (in the time interval of 15-75 min) than their pure counterpart (2-15%).

Keywords: Cerium oxide, Nanoparticles, Calcium-doping, Adsorption, Photocatalytic activity.

INTRODUCTION

Cerium belongs to the lanthanide series, which is most abundant rare earth element [1]. Cerium has great demand due to its broad application in the chemical-mechanical polishing field [2], as oxygen gas sensor [3] and UV absorbent [4]. There are few studies on investigation of the effective adsorption of heavy metal ions like Cr^{6+}, Pb^{2+}, Cd^{2+}, *etc*. by CeO_2 NPs [5] and hence these methods can be utilized in elimination of heavy metals and other impurities from the water bodies. In several works [6,7], doping of CeO_2 NPs with Zn, Mg and Ca has been successfully attempted, in order to shift the material's band-gap value and thereby modify the electronic transitions [8]. Another important application of CeO_2 and doped CeO_2 NPs is their photocatalytic activity [9-11]. For photocatalytic degradation activity to work ideally, a potential photocatalyst should have the ideal bandgap of a semiconducting material like ZnO, CeO_2, TiO_2 or Cu_2O [12]. For this reason, it would be beneficial to dope CeO_2 NPs with various metal ions to alter its bandgap and then investigate the photocatalytic activity of the synthesized nanoparticles.

Additionally, CeO_2 alone in cosmetics has reportedly been shown to be unsuitable due to its strong catalytic activity [13]. Ideally, the ionic radius ratio for fluorite-type structures should be 0.732 in an octahedron MO_8. Due to the tiny ionic radius of Ce^{4+}, the fluorite structure of CeO_2 is unstable and cannot attain the ideal ionic radius ratio value of 0.732. Consequently, Ce^{4+} ions have a natural inclination to become Ce^{3+} ions (which has a larger ionic radius) to stabilize the system. The conversion of Ce^{4+} to Ce^{3+} is accompanied by release of oxygen in order to neutralize the charges. This leads to negative effects such as oxidation of organic molecules present in the CeO_2 containing sunscreens. Doping of Ca^{2+} ions in CeO_2 NPs helps in the replacement of Ce^{4+} by a cation with a lower valence and a larger ionic radius and thereby gives stability to the fluorite structure [14]. Further, it is reported that the dissolution of Ca^{2+} ions in the metal oxide lattice helps in decreasing the hydraulic radii and increasing the surface area (S_{BET}) and total pore volume (V_P) of the prepared oxide samples [15]. Therefore, in addition to modification of the bandgap and offering stability to the fluorite structure of CeO_2, doping of CeO_2 by Ca^{2+} also improves

the ability of CeO_2 to act as a better adsorbent. This was substantiated by carrying out the adsorption studies of both CeO_2 and calcium doped CeO_2 NPs in the present work. Various chemical methods are adopted for the synthesis of pure and doped CeO_2 NPs. Among them, the electrochemical deposition [16], hydrothermal synthesis [17,18], sol-gel [19,20] and the co-precipitation [21,22] are the important ones. The co-precipitation method has some benefits, such as, it is elementary, economical and gives repeatable results.

Although previous studies report the effects of Ca^{2+} doping on CeO_2 nanoparticles [12], no attempt has been earlier made to study the effect of Ca^{2+} doping on adsorption behaviour and photocatalytic activities of CeO_2 NPs. Therefore, in present work, the synthesis and characterization of Ca^{2+} doped CeO_2 NPs is reported. Co-precipitation method was employed for the synthesis of nanoparticles and the XRD, SEM, EDX studies were carried out for characterization. The results of adsorption and photocatalytic activity studies are also reported herein.

EXPERIMENTAL

Synthesis of pure cerium oxide nanoparticles: Pure CeO_2 NPs were prepared by the precipitation method. In brief, ammonium ceric sulfate dihydrate (0.3163 g, 0.5 mmol) was dissolved in 2 M H_2SO_4 (50 mL) followed by the addition of 5 mL of ethanol and then the resulting mixture was heated with stirring up to 50 ºC. After 30 min of stirring, a pale-yellow dispersion was obtained which was then further heated with stirring at 50 ºC for 4 h. The obtained pale-yellow coloured precipitate was filtered, washed with 100 mL of water and 25 mL of ethanol and dried at 200 ºC for 2 h.

Synthesis of Ca^{2+}-doped CeO_2 NPs: Calcium doped CeO_2 NPs were prepared by adding calcium chloride (0.04 M, 20 mL) to a solution of ammonium ceric sulphate (50 mL) and a similar procedure was employed as mentioned above.

Characterization: Crystallinity and particle size of nanoparticles were determined by using XRD studies [23]. The phase formation and crystallinity were examined using powder X-ray diffraction (XRD, Bruker miniflex 600 model). The size of the nanoparticles was determined by using 2θ values. SEM images of pure and doped CeO_2 nanoparticles were used to examine the surface morphology of the nanoparticles present in the sample. They were further characterized using the EDX technique to determine the percentage composition of various elements present in the sample. The morphology and structure of Ca^{2+} doped CeO_2 NPs surface were analyzed with scanning electron microscope EDAX (SEM, Zeiss EVO18 special edition) and the morphology and structure of pure CeO_2 NPs surface were analyzed with scanning electron microscope EDAX (SEM, Hitachi S3500). Optical transmittances of the pure and Ca^{2+} doped CeO_2 nanoparticles were studied by UV-visible double beam spectrophotometer (Systronics 2202) in the range of 200-800 nm.

BET analysis: Determination of the effective surface area of the nanoparticles is a prerequisite to study their adsorption behaviour [24]. The physical adsorption of gas molecules on a solid surface is explained by the BET theory, which also forms the basis for calculating the specific surface area of materials. Adsorption studies were made using Quantachrome Instrument (Version 3.0, USA), by using nitrogen gas as gaseous adsorbate at 77 K.

Adsorption studies: A 50 mL of chitosan solution (500 ppm) was added to each of the two bottles containing 0.1 g each of pure CeO_2 and Ca^{2+} doped CeO_2 nanoparticles were dispersed with the help of a sonicator. Then, 6 mL of methylene blue solution (2 g/dm^3, 6 mmol) was added to each bottle and each solution was diluted to 100 mL using distilled water. Each mixture was operated using electrically operated rotary shaker for 10 min (at 100 rpm) for uniform mixing. The pH of each solution was adjusted to 3 by adding HCl dropwise. Then each solutions were again subjected to uniform mixing by using the rotary shaker for 10 min (at 100 rpm) and pH of each solution was brought to 10 by adding NaOH dropwise. Each solution were thoroughly shaken for further 10 min and kept aside for the solidified chitosan to settle down. After a predetermined time (0 to 75 min, regular time interval), the solution was filtered and the absorbance of the filtrate was measured using the UV-visible spectrophotometer. The concentration of unadsorbed CeO_2 in the filtrate was found out by redox titration against 0.05 M Mohr's salt solution using Ferroin indicator. The concentration of Ce(III) determined by titrimetric method was found to be negligible.

Photocatalytic activity: Weighed exactly 0.1 g of pure CeO_2 NPs and transferred into a pyrex glass beaker containing methyl orange solution (1 ppm). The solid nanoparticles were dispersed in the dye solution for 5 min. Further, to achieve adsorption-desorption equilibrium in these studies, methyl orange solution containing the photocatalyst in the pyrex glass beaker was magnetically agitated for 30 min. The entire solution was kept under dark condition during agitation. Then, 7 mL of sample from the container was collected through syringe, nanoparticles were separated by centrifugation and the change of absorbance of the dye was monitored by UV-vis spectrophotometer (a_0). The same procedure was followed for the Ca^{2+} doped CeO_2 nanaparticles too.

RESULTS AND DISCUSSION

XRD studies: In XRD analysis, the size of the synthesized nanoparticles, D, was calculated by using the Schrerrer's equation [25]:

$$D = \frac{K\lambda}{(\beta \cos\theta)} \quad (1)$$

where K is a constant whose value depends on the crystallite shape (a good approximate is K = 0.9), β is the full width at the half maximum (FWHM) which is obtained from the spectra using the Origin 9 software, θ is the diffraction angle (in radians) and λ is the wavelength.

The XRD patterns of pure and Ca^{2+} doped CeO_2 NPs (40 mol% doped) are shown in Fig. 1. The samples are in single-phase and consist of the fluorite type cubic structure CeO_2 phase. The crystallite sizes were calculated from the most intense peaks (2θ) by using eqn. 1. The size of the prepared Ca^{2+} doped CeO_2 NPs and pure CeO_2 NPs was found to be 2 nm (2θ = 28.52º) and 9.3 nm (2θ = 38.24º), respectively [26] [JCPDS-

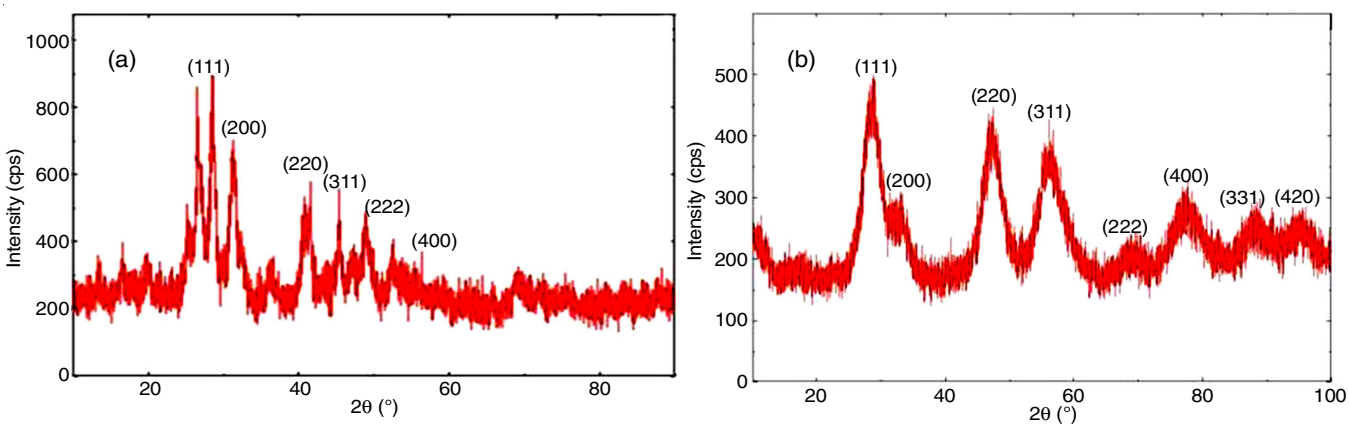

Fig. 1. XRD patterns of pure CeO_2 (a) and Ca^{2+} doped CeO_2NPs (b)

0004-0593]. Using combustion method, the size of the synthesized pure CeO_2 NPs was found to be 35 nm [27], whereas the size of cobalt- doped CeO_2 NPs was 5-8 nm [28].

In this study, the XRD peaks of Ca^{2+} doped CeO_2NPs are broadened due to its amorphous nature. The finite size of the crystals causes the peaks of the XRD patterns to broaden. The peaks in the XRD pattern will be extremely sharp if the crystal is infinitely large and as the crystal gets smaller, peak broadening will become more pronounced. Moreover, it has been observed that on increasing the doping concentration from 0 to 50% (in the increment of 10%) decreased the size of nanoparticles from 9.3 nm (for 0%) to 5.7 nm (for 50%). The decrease in particle size with increase in doping percentage was not uniform. The decrease in size with doping was very fast upto 30 mol%, beyond which the decrease is very slow-almost reaching saturation near 50 mol% [26]. Though pure and Ca^{2+} doped CeO_2 NPs were prepared by co-precipitation method, a significant difference in the nanoparticles sizes is reported in literature (around 5.7 nm) [26]. This may be due to the difference in the source of cerium ions used in the synthesis. In present work, during synthesis of nanoparticles, Ce^{4+} was used directly (in the form of ceric ammonium sulphate solution), while in the literature work, the synthesis of nanoparticles involved an *in situ* oxidation of Ce^{3+} (taken in the form of ceric nitrate solution) to Ce^{4+} by using hydrogen peroxide.

SEM studies: The shape of pure CeO_2 NPs is not clear in its SEM image (Fig. 2a), which is attributed due to the agglomeration. However, agglomeration of nanoparticles was reduced to some extent after doping with Ca^{2+}. The SEM images of Ca^{2+} doped CeO_2 NPs (Fig. 2b) shows the presence of spherical shaped nanoparticles [29,30]. The size of pure CeO_2 NPs was found to be in between 5-9 nm, while that of Ca^{2+} doped CeO_2 NPs was found to be in the range of 1-4 nm.

EDX studies: The EDX spectra of pure and 40 mol% Ca^{2+} doped-CeO_2 NPs are shown in Fig. 3a-b, respectively. Compared to pure CeO_2 NPs, the EDX pattern of doped sample shows the significant peaks, which is due to the contribution from Ca in addition to other peaks from elements such as Ce and O, thereby confirming the doping of Ca^{2+} into CeO_2 NPs.

BET surface studies: The pore size, pore diameter and surface area of the prepared Ca^{2+} doped-CeO_2 NPs (40 % doping) were investigated using BET surface analysis. The adsorption-

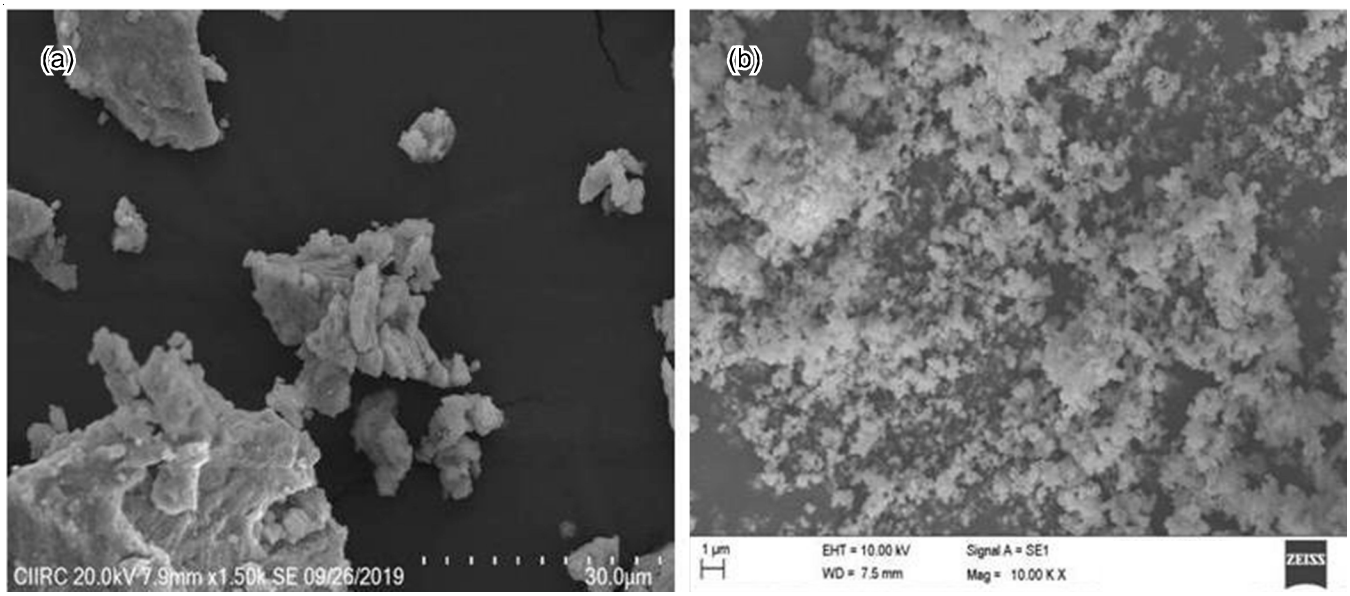

Fig. 2. SEM images of pure CeO_2 (a) and Ca^{2+} doped CeO_2NPs (b)

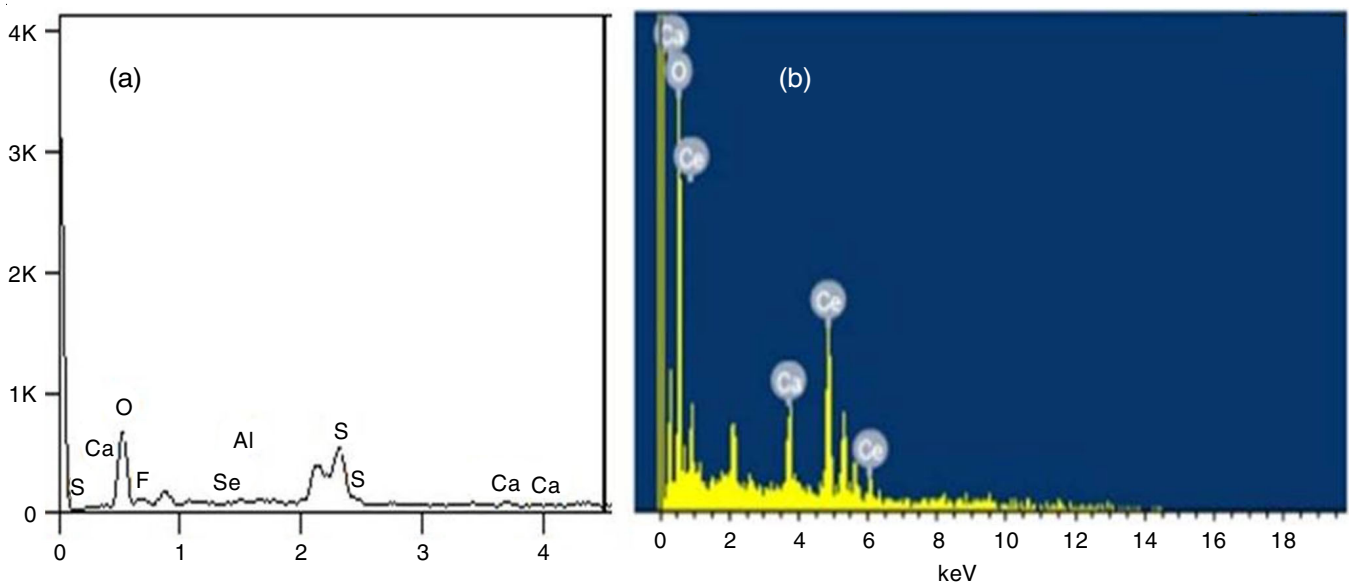

Fig. 3. EDX spectra of pure CeO_2 NPs (a) and Ca^{2+} doped-CeO_2 NPs (b)

desorption isotherms of Ca^{2+} doped-CeO_2 NPs doped samples were analyzed using a static volumetric adsorption analyzer. Fig. 4a shows the N_2 adsorption-desorption BET isotherm, while, Fig. 4b displays the Barret-Joyner-Halenda (BJH) pore size distribution plot for Ca^{2+} doped-CeO_2 NPs. The adsorption-desorption isotherm is a hysteresis loop exhibiting type IV pattern as recommended by IUPAC.

From the literature, the average surface area, pore volume and pore diameter of CeO_2 NPs prepared by different methods were found to be in the range of 30-40 m^2/g, 0.2-0.3 cm^3/g and 50-100 Å, respectively [27,31]. However, CeO_2 NPs prepared by the solution combustion method [27] and self-assembly of NPs in liquid crystal phase [32] have reported much higher surface area of 163.5 m^2/g and 125 m^2/g, respectively. The specific surface area of Ca^{2+} doped CeO_2 NPs were calculated using the BET-equation. In present study, Ca^{2+} doped-CeO_2 NPs had a surface area of 59.806 m^2/g, which is more than 10-fold higher than that of bulk CeO_2 (5.67 m^2/g) and higher than that of pure CeO_2 NPs (30-40 m^2/g) prepared by most of the methods [33]. As a result, Ca^{2+} doped CeO_2 NPs were expected to have better adsorption capacities than pure CeO_2 NPs. In BET analysis, the pore volume and the pore diameter of Ca^{2+} doped CeO_2 NPs were found to be 0.236 cm^3/g and 150 Å, respectively.

Adsorption studies: In this study, the effect of pure and Ca^{2+} doped CeO_2 NPs on the efficiency of chitosan to adsorb methylene blue dye was carried out. It was observed that as pH increases, the adsorption of the dye decreases. However, as methylene blue is a cationic dye, it can be better adsorbed on the anionic chitosan at higher pH 10 [31]. At pH 10, the amines in the chitosan are deprotonated and are present in the insoluble form represented as follows:

$$\text{Chitosan} - NH_2 + OH^- + H_2O \longrightarrow \text{Chitosan} - NH_2^- + 2H_2O$$

After adsorption, at different time intervals (0-75 min), the remaining solution was centrifuged at a speed of 17300 rpm. The absorbance of the supernatant solution was found out by using UV visible spectrophotometer. On comparing the absorbance of the solution containing chitosan decorated Ca^{2+} doped-CeO_2 NPs with that of the solution containing chitosan decorated undoped CeO_2 NPs, a decrease in absorbance of dye was observed in the former. According to

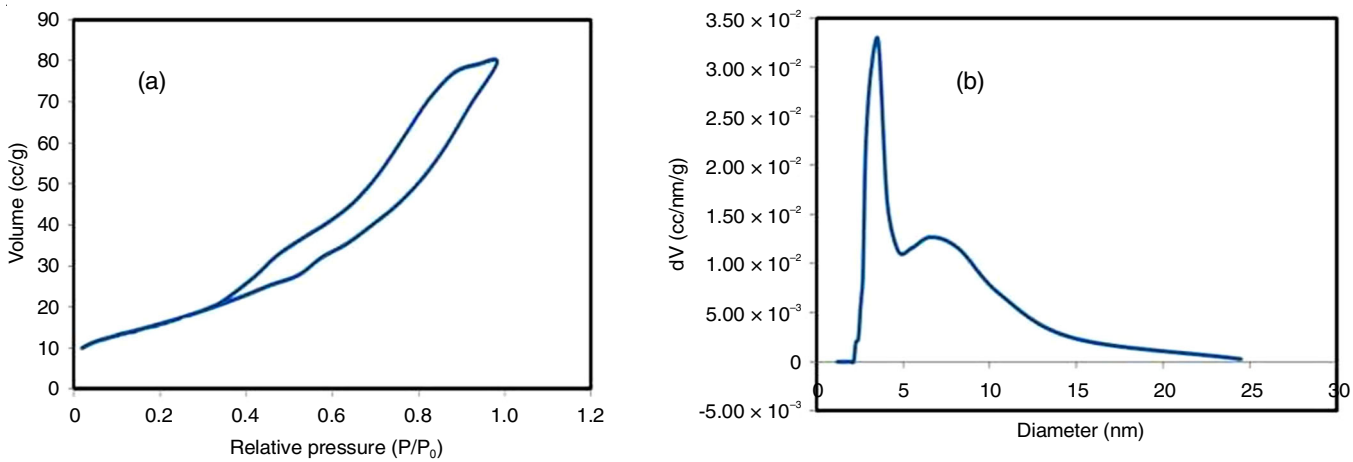

Fig. 4. BET adsorption-desorption isotherm (a) and pore size distribution plot for Ca^{2+} doped-CeO_2 NPs (b)

Beer-Lambert's law, absorbance is directly proportional to the dye concentration; a decrease in absorbance therefore refers to decrease in concentration of the dye in the solution [34]. This indicates that Ca^{2+} doped CeO_2 NPs improve the adsorption efficiency of chitosan to a greater extent than the pure CeO_2 NPs. The percentage removal of dye using chitosan decorated bare an Ca^{2+} doped CeO_2 NPs was calculated by using the following equation [35]:

$$\text{Removal of dye (\%) } Q = \frac{\alpha_o - \alpha}{\alpha_o} \times 100$$

where α_o and α are the initial and final absorbance.

The percentage of the adsorption of dye (Q) on the chitosan incorporated with Ca^{2+}/CeO_2 NPs is more than the bare CeO_2 NPs at various time intervals (0-75 min) (Fig. 5).

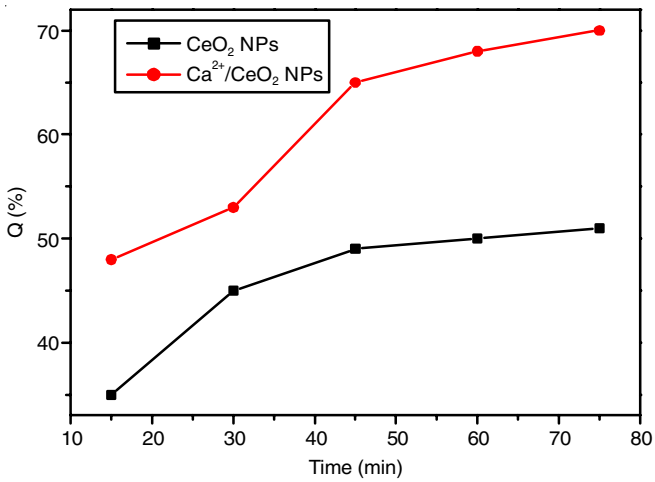

Fig. 5. Percentage of adsorption of the dye (Q) on chitosan incorporated with CeO_2 NPs and Ca^{2+}/CeO_2 NPs

The reason for this enhancement may be due to increase in the adsorbent's surface area aided by the NPs [10,36]. As the Ca^{2+} doped CeO_2 NPs have greater surface area than the undoped ones, this justifies the greater efficiency of chitosan in removal of dye in the presence of Ca^{2+} doped CeO_2 NPs. This is further supported by the observation that percentage of adsorption in the presence of undoped CeO_2 NPs reaches a saturation at greater time intervals, while, there is still a steady increase in percentage adsorption even at greater time intervals in the presence of Ca^{2+} doped CeO_2 NPs.

Photocatalytic activity: The photocatalytic properties of synthesized Ca^{2+} doped CeO_2 NPs were studied by using methyl orange dye. The study showed that the performance of Ca^{2+} doped CeO_2 NPs in the photocatalytic degradation of methyl orange was higher compared to pure CeO_2 NPs. The nanoparticle degrades the dye in the presence of light [37] and as a result, the concentration of dye gets decreased. The percentage degradation of dye was investigated by employing a UV-visible spectrophotometer. From UV-visible absorption spectra, it was observed that on increasing the time interval the absorbance decreases (Fig. 6) and therefore, the percentage of dye degradation increases with time.

It was found that the photocatalytic activity of dye degradation of pure CeO_2 NPs and Ca^{2+} doped CeO_2 NPs was found

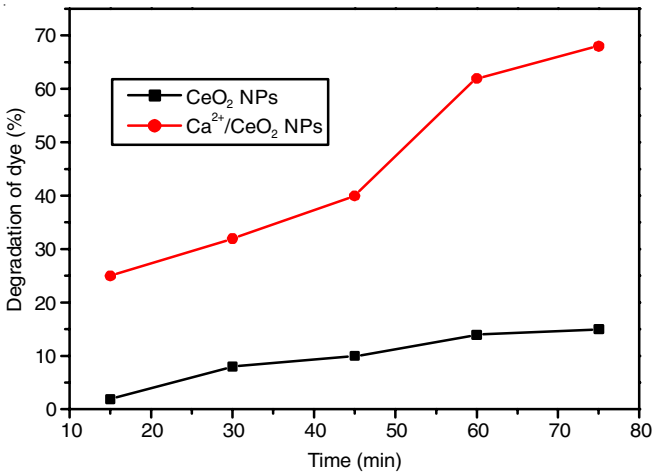

Fig. 6. Comparison of photocatalytic degradation of methyl organe dye (%) in the presence of visible light by CeO_2 NPs and Ca^{2+}/CeO_2 NPs (40% doping)

to be 15% and 68%, respectively (Fig. 6). The enhancement in the photocatalytic degradation efficiency of CeO_2 NPs upon calcium doping may be due to an increase in the charge transport rate [38].

Mechanism of photocatalytic degradation: Energy band gap is one of the important factors that is considered during assessment of any material for its photocatalytic activity. CeO_2 NPs display a wide range of energy band gap of 2.6-3.4 eV [39,40]. The energy band gap may be fine tuned or modulated by modifying the preparative methods and it can be improved by doping NPs with transition metal ions [41,42]. Doping may result in lattice defects formation, which may alter the electronic structure by better electron-hole charge separation, leading to greater efficiency of the material to absorb visible light [42,43]. Due to the increase of charge separation *i.e.* separation of electrons and holes facilitated by Ca^{2+}, Ca^{2+} doped CeO_2 NPs have greater photocatalytic efficiency than the undoped ones. Also, the fact that Ca^{2+} doped CeO_2 NPs offers larger specific surface area giving more reaction sites and stronger adsorption capacity for the dye molecules results in further enhancement of photocatalytic activity [44,45].

Conclusion

The synthesized Ca^{2+} doped CeO_2 NPs were characterized by using XRD, SEM, EDX and BET surface analysis. The synthesized nanoparticles have fluorite type cubic structure with particle size of 2 nm, which is less than that observed for undoped NPs *viz*. 9 nm. SEM images revealed that Ca^{2+} doped CeO_2 NPs have regular spherical shapes, while the undoped CeO_2 NPs do not have a regular shape due to agglomeration. Comparison of EDX profiles of doped and undoped nanoparticles showed the presence of additional peak due to calcium in the EDX profile of doped nanoparticles, in addition to those of cerium and oxygen, thereby confirming successful doping. From BET analysis, it was observed that the surface area of doped CeO_2 NPs is much greater than that of pure CeO_2 NPs synthesized by different methods. Adsorption studies revealed that Ca^{2+} doped CeO_2 NPs offer larger surface area than the undoped ones and therefore, the presence of the former enhances

the adsorption capacity towards the dye removal efficiency of chitosan incorporated doped rare earth metal oxide nanoparticles. The photocatalytic studies revealed that Ca^{2+} doped CeO_2 NPs are much better and potential candidate for the photocatalytic degradation of methyl orange dye than undoped CeO_2 NPs. The higher efficiency of Ca^{2+} doped CeO_2 NPs is because of the efficient charge separation of electrons and holes offered by Ca^{2+} ions.

ACKNOWLEDGEMENTS

The authors are thankful to UGC for the financial assistance given in the form of Major research project MRP-MAJOR-CHEM-2013-44460.

CONFLICT OF INTEREST

The authors declare that there is no conflict of interests regarding the publication of this article.

REFERENCES

1. G. Renu, V.V. Rani, S.V. Nair, K.R.V. Subramanian and V.K. Lakshmanan, *Adv. Sci. Lett.*, **6**, 17 (2012); https://doi.org/10.1166/asl.2012.3312
2. P. Janoš, J. Ederer, V. Pilarová, J. Henych, J. Tolasz, D. Milde and T. Opletal, *Wear*, **362-363**, 114 (2016); https://doi.org/10.1016/j.wear.2016.05.020
3. T.T. Phan, T. Tosa and Y. Majima, *Sens. Actuators B Chem.*, **343**, 130098 (2021); https://doi.org/10.1016/j.snb.2021.130098
4. N. N. Dao, M. D. Luu, Q. K. Nguyen and B. S. Kim, *Adv. Nat. Sci.: Nanosci. Nanotechnol.*, **2**, 045013 (2011); https://doi.org/10.1088/2043-6262/2/4/045013
5. A.R. Contreras, E. Casals, V. Puntes, D. Comilis, A. Sanchez and X. Font, *Glob. NEST J.*, **17**, 536 (2015); https://doi.org/10.30955/gnj.001687
6. I.A. Siddiquey, T. Furusawa, Y.I. Hoshi, E. Ukaji, F. Kurayama, M. Sato and N. Suzuki, *Appl. Surf. Sci.*, **255**, 2419 (2008); https://doi.org/10.1016/j.apsusc.2008.07.112
7. B.G. Pound, *Solid State Ion.*, **52**, 183 (1992); https://doi.org/10.1016/0167-2738(92)90104-W
8. S. Tsunekawa, T. Fukuda and A. Kasuya, *J. Appl. Phys.*, **87**, 1318 (2000); https://doi.org/10.1063/1.372016
9. A. Akbari-Fakhrabadi, R. Saravanan, M. Jamshidijam, R.V. Mangalaraja and M.A. Gracia, *J. Saudi Chem. Soc.*, **19**, 505 (2015); https://doi.org/10.1016/j.jscs.2015.06.003
10. J. Saranya, K.S. Ranjith, P. Saravanan, D. Mangalaraj and R.T. Rajendra Kumar, *Mater. Res. Semiconduct. Process.*, **26**, 218 (2014); https://doi.org/10.1016/j.mssp.2014.03.054
11. J. Huang, F. Chen, H. Wang and H. Yan, *Res. Chem. Intermed.*, **44**, 2729 (2018); https://doi.org/10.1007/s11164-018-3257-8
12. A. Syed, L.S.R. Yadav, A.H. Bahkali, A.M. Elgorban, D. Abdul Hakeem and N. Ganganagappa, *Crystals*, **10**, 817 (2020); https://doi.org/10.3390/cryst10090817
13. A. Zenerino, T. Boutard, C. Bignon, S. Amigoni, D. Josse, T. Devers and F. Guittard, *Toxicol. Rep.*, **2**, 1007 (2015); https://doi.org/10.1016/j.toxrep.2015.07.003
14. K.K. Babitha, A. Sreedevi, K.P. Priyanka, B. Sabu and T. Varghese, *Indian J. Pure Appl. Phys.*, **53**, 596 (2015).
15. N.-A.M. Deraz, *Adsorpt. Sci. Technol.*, **21**, 229 (2003); https://doi.org/10.1260/026361703322404386
16. R. Murugan, G. Ravi, R. Yuvakkumar, S. Rajendran, N. Maheswari, G. Muralidharan and Y. Hayakawa, *Ceramics Int.*, **43**, 10494 (2017); https://doi.org/10.1016/j.ceramint.2017.05.096
17. M. Radovic, Z.D. Dohcevic-Mitrovic, A. Golubovic, B. Matovic, M. Šcepanovic and Z.V. Popovic, *Acta Phys. Polon. A*, **116**, 614 (2009).
18. P. Mukherjee, A. Ahmad, D. Mandal, S. Senapati, S.R. Sainkar, M.I. Khan, R. Parishcha, P.V. Ajaykumar, M. Alam, R. Kumar and M. Sastry, *Nano Lett.*, **1**, 515 (2001); https://doi.org/10.1021/nl0155274
19. E.K. Goharshadi, S. Samiee and P. Nancarrow, *J. Colloid Interface Sci.*, **356**, 473 (2011); https://doi.org/10.1016/j.jcis.2011.01.063
20. S.S. Behera, J.K. Patra, K. Pramanik, N. Panda and H. Thatoi, *World J. Nano Sci. Eng.*, **2**, 196 (2012); https://doi.org/10.4236/wjnse.2012.24026
21. G. Killivalavan, A.C. Prabakar, K.C. Babu Naidu, B. Sathyaseelan, G. Rameshkumar, D. Sivakumar, K. Senthilnathan, E. Manikandan, I. Baskaran and B. Ramakrishna Rao, *Biointerf. Res. Appl. Chem.*, **10**, 5306 (2020); https://doi.org/10.33263/BRIAC102.306311
22. D.M. Prabaharan, K. Sadaiyandi, M. Mahendran and S. Sagadevan, *Mater. Res.*, **19**, 478 (2016); https://doi.org/10.1590/1980-5373-MR-2015-0698
23. C.R. Martin, *Nanomedicine*, **1**, 5 (2006); https://doi.org/10.2217/17435889.1.1.5
24. V.D. Kosynkin, A.A. Arzgatkina, E.N. Ivanov, M.G. Chtoutsa, A.I. Grabko, A.V. Kardapolov and N.A. Sysina, *J. Alloys Compd.*, **303-304**, 421 (2000); https://doi.org/10.1016/S0925-8388(00)00651-4
25. C. Hu, Z. Zhang, H. Liu, P. Gao and Z.L. Wang, *Nanotechnology*, **17**, 5983 (2006); https://doi.org/10.1088/0957-4484/17/24/013
26. L. Truffault, M.-T. Ta, T. Devers, K. Konstantinov, C. Simmonard, V. Harel, C. Andreazza, I.P. Nevirkovets, A. Pineau, O. Veron and J.-P. Blondeau, *Mater. Res. Bull.*, **45**, 527 (2010); https://doi.org/10.1016/j.materresbull.2010.02.008
27. T.N. Ravishankar, T. Ramakrishnappa, G. Nagaraju and H. Rajanaika, *ChemistryOpen*, **4**, 146 (2015); https://doi.org/10.1002/open.201402046
28. J. Saranya, K.S. Ranjith, P. Saravanan, D. Mangalaraj and R.T. Rajendra Kumar, *Mater. Sci. Semicond. Process.*, **26**, 218 (2014); https://doi.org/10.1016/j.mssp.2014.03.054
29. M. Kumari, M. Kumar, A. Kumar, S. Kumara and D. Kumar, Synthesis of Lithium Doped Cerium Oxide Nanoparticle by the Co-precipitation Method, In: Recent Trends in Materials and Devices, Conference Proceedings, pp. 131-137 (2017).
30. J. Kaspar, P. Fornasiero and M. Graziani, *Catal. Today*, **50**, 285 (1999); https://doi.org/10.1016/S0920-5861(98)00510-0
31. I.I. Soykal, H. Sohn, B. Bayram, P. Gawade, M.P. Snyder, S.E. Levine, H. Oz and U. Ozkan, *Catalysts*, **5**, 1306 (2015); https://doi.org/10.3390/catal5031306
32. J.-Y. Chane-Ching, F. Cobo, D. Aubert, H.G. Harvey, M. Airiau and A. Corma, *Chem. Eur. J.*, **11**, 979 (2005); https://doi.org/10.1002/chem.200400535
33. C. Pan, D. Zhang and L. Shi, *J. Solid State Chem.*, **181**, 1298 (2008); https://doi.org/10.1016/j.jssc.2008.02.011
34. V. Ramasamy, V. Mohana and G. Suresh, *Int. J. Mater. Sci.*, **12**, 79 (2017).
35. A. Stambouli and E. Traversa, *Renew. Sustain. Energy Rev.*, **6**, 433 (2002); https://doi.org/10.1016/S1364-0321(02)00014-X
36. S. Rajeshkumar and P. Naik, *Biotechnol. Rep.*, **17**, 1 (2018); https://doi.org/10.1016/j.btre.2017.11.008
37. A. Kumar, M. Kumari, M. Kumar, S. Kumar and D. Kumar, *AIP Conf. Proc.*, **1728**, 020444 (2016); https://doi.org/10.1063/1.4946495
38. H.I. Chen and H.Y. Chang, *Ceram. Int.*, **31**, 795 (2005); https://doi.org/10.1016/j.ceramint.2004.09.006
39. E.A. Kusmierek, *Catalysts*, **10**, 1435 (2020); https://doi.org/10.3390/catal10121435
40. B. Choudhury, P. Chetri and A. Choudhury, *J. Exp. Nanosci.*, **10**, 103 (2015); https://doi.org/10.1080/17458080.2013.801566
41. P.P. Ortega, B. Hangai, H. Moreno, L.S.R. Rocha, M.A. Ramírez, M.A. Ponce, E. Longo and A.Z. Simões, *J. Alloys Compd.*, **888**, 161517 (2021); https://doi.org/10.1016/j.jallcom.2021.161517
42. Y. Qi, J. Ye, S. Zhang, Q. Tian, N. Xu, P. Tian and G. Ning, *J. Alloys Compd.*, **782**, 780 (2019); https://doi.org/10.1016/j.jallcom.2018.12.111
43. R. Ma, S. Zhang, T. Wen, P. Gu, L. Li, G. Zhao, F. Niu, Q. Huang, Z. Tang and X. Wang, *Catal. Today*, **335**, 20 (2019); https://doi.org/10.1016/j.cattod.2018.11.016
44. L. Zhu, H. Li, P. Xia, Z. Liu and D. Xiong, *ACS Appl. Mater. Interfaces*, **10**, 39679 (2018); https://doi.org/10.1021/acsami.8b13782
45. S. Rajendran, M.M. Khan, F. Gracia, J. Qin, V.K. Gupta and S. Arumainathan, *Sci. Rep.*, **6**, 31641 (2016); https://doi.org/10.1038/srep31641